Energy 268 (2023) 126632

Contents lists available at ScienceDirect

Energy

journal homepage: www.elsevier.com/locate/energy

Performance variations of wave energy converters due to global long-term wave period change (1900–2010)

Alain Ulazia [a,*], Aitor Saenz-Aguirre [a], Gabriel Ibarra-Berastegui [b,c], Jon Sáenz [d,c], Sheila Carreno-Madinabeitia [e], Ganix Esnaola [a,c]

[a] Energy Engineering Department, University of the Basque Country (UPV/EHU), Otaola 29, 20600 Eibar, Spain
[b] Energy Engineering Department, University of the Basque Country (UPV/EHU), Alda. Urkijo, 48013 Bilbao, Spain
[c] Plentziako Itsas Estazioa (BEGIK), University of the Basque Country (UPV/EHU), Areatza Hiribidea 47, 48620 Plentzia, Spain
[d] Department of Physics, University of the Basque Country (UPV/EHU), Sarriena Auzoa, 48940 Leioa, Spain
[e] Department of Mathematics, University of the Basque Country (UPV/EHU), Paseo de la Universidad, 01006, Vitoria-Gasteiz, Spain

ARTICLE INFO

Keywords:
Wave energy
Wave period
Oscillating water column
Long-term wave energy trends

ABSTRACT

Long-term ocean climate effects on wave energy are often analysed from the viewpoint of the well-known increment of wave height over the decades. However, this increment associated with the increase of wave energy flux and absorbed power does not consider the influence of variations in the wave period, whose contribution is more important according to an adimensional performance analysis given by the capture width ratio. This study identifies significant past variations in wave periods during the 20th and 21st centuries using the reanalysis ERA-20C globally and at specific locations, such as Ireland, via calibration with ERA5. A more specific analysis developed in this area shows very significant performance variations (up to 20%) for two types of wave energy converters: oscillating water column devices and a floating body, in which laboratory empirical equations have been used to compute their performance loss due to the deviation from its natural resonance frequency or optimum working wave period. Thus, the performance measured as capture width ratio is highly sensitive to wave period changes, even losing productivity for regions where the wave energy potential is being incremented during the last decades.

1. Introduction

Decarbonisation of the energy sector is one of the most important future actions of humanity in the coming decades to weaken the impact of greenhouse gas emissions (GHGEs), as two-thirds of all GHGEs stem from energy production [1]. The renewable share of the total energy supply should therefore be drastically increased, which would also involve other socio-economic benefits [2]. Hence, apart from the well-known solar and onshore wind energy sources, less developed technologies such as wave energy will also play an important role [3].

Although advances in wave energy converters still face survivability, maturity, and cost challenges, different types of technological synergies can accelerate their real implementation in the near future. The synergy between ocean wind and wave energy based on renewable energy production, or the synergy between wave energy farms and coastal protection according to mitigation of global warming effects on the shoreline, both constitute promising co-lateral innovations in favour of wave energy conversion technologies (WECs) [4–6].

The synergy of wave energy with coastal mitigation effects contains a fundamental aspect that requires long-term analysis of the resource according to climate change. Several studies have already shown a general increase in wave height and energy worldwide using past data and future projections via the Coupled Model Intercomparison Project Phases 5 and 6 (CMIP5 and CMIP6). Thus, a global average annual increment of 0.4% has been identified since 1948 for wave power, finding long-term correlations with sea surface temperatures, which indicates that global warming is making waves stronger [7].

The Southern Ocean defined between latitudes of 40°S and 80°S presents the highest changes increasing in the past 50 years from a spatial average wave power of around 310^5 kW/m to almost 510^5 kW/m [7]. For specific grid points, differences in the mean wave power during the decade of 1991–2000 with respect to the mean value in 1981–1990 have reached 30 kW/m in the south of Australia, Chile, and South Africa [8], which constitutes a huge value than can increment the available power by 30%–40% in these sites. For future

* Corresponding author.
E-mail addresses: alain.ulazia@ehu.eus (A. Ulazia), aitor.saenz@ehu.eus (A. Saenz-Aguirre), gabriel.ibarra@ehu.eus (G. Ibarra-Berastegui), jon.saenz@ehu.eus (J. Sáenz), sheila.carreno@ehu.eus (S. Carreno-Madinabeitia), ganix.esnaola@ehu.eus (G. Esnaola).

https://doi.org/10.1016/j.energy.2023.126632
Received 16 September 2022; Received in revised form 30 November 2022; Accepted 5 January 2023
Available online 10 January 2023

List of Abbreviations

AMETS	Atlantic Marine Energy Test Site
BEM	Boundary Element Method
FB	Floating Body
CMIP5	Coupled Model Intercomparison Project Phase 5
CMIP6	Coupled Model Intercomparison Project Phase 6
ECMWF	European Centre for Medium-Range Weather Forecasts
ENSO	El Ni o
ERA-20C	ECMWF's 20th century reanalysis
ERA5	ECMWF's 5th reanalysis
GHGEs	Greenhouse Gas Emissions
ICOADS	International Comprehensive Ocean-Atmosphere Data
ISPD	International Surface Pressure Databank
OWC	Oscillating Water Column
O-FB	Oscillating Floating Body by Oigarden and Olsen
PTO	Power Take-Off
RCP	Representative Concentration Pathways
SAM	Southern Annular Mode
SWAN	Simulating Waves Nearshore
SSP	Shared Socioeconomic Pathway
WEC	Wave Energy Converter

Nomenclature

a, b, c, d, f	Results of empirical equations
B	OWC Cavity length (m)
CW	Capture Width (m)
CWR	Capture Width Ratio
CWR_{fb}	CWR of the floating body
CWR_{OWC}	CWR of the OWC
D	OWC Cavity draught (m)
D_x	Adimensional draught
H_s	Significant wave height
h_x	Relative depth
h	Depth (m)
K	Damping coefficient (Ns/m)
k	Wave number (m^{-1})
K_x	Adimensional damping
P_{abs}	Absorbed power (kW)
P_{wave}	Wave energy flux (kW/m)
P_i, Q_i	$i \in \{1, 14\}$ Empirical numerical parameters
T_p	Peak wave period (s)
T_m	Mean wave period (s)
T_e	Energy period (s)
W	OWC Cavity width (m)
W_x	Adimensional width
WEF	Wave Energy Flux (kW/m)
λ	Wave length (m)
ρ_a	Air density (kg/m^3)

projections of wave extremes using CMIP5, the Southern Ocean is again the area with the highest increment in extreme waves [9]. These trends have been corroborated using different data sources such as satellites [10], in-situ measurements [11], and visual observations [12], observing, for instance, an increment of approximately 5 cm/decade in the North Atlantic. Furthermore, several authors have already shown a general increment of wave height and, therefore, wave energy, around the planet using past data and future projections via Coupled Model Intercomparison Project Phase 5 and 6 (CMIP5 and CMIP6) [13].

The effects of these historical increments on the energy production of different wave energy converters have been analysed by the authors in Ireland [14], Chile [15], Iceland [16] or Gulf of Biscay [17] using reanalysis data of ERA-20C (last century) calibrated against ERA-Interim. In these previous cases, significant wave height (Hs) or directly Wave Energy Flux (WEF) were analysed according to their trends and historical evolution, introducing them in the energy capture hydrodynamic models of different WECs.

However, very few specific studies on wave period can be found in the literature [18–22], and most do not show a long-term study on the historical trends, with the exception of [23], which shows an interesting hemispheric asymmetry of future wave trends: North Hemisphere shows an slow decreasing trend of wave period, while the Southern Ocean increases its period mainly during the austral winter. CMIP5 projections also confirm the different behaviour of the wave period in both hemispheres during the 21st Century [23,24]. A similar asymmetry for the peak period has also been reported in the literature [25]. Changes in different wave parameters, including mean wave period seem to be driven by large circulation patterns like El Niño (ENSO) and the Southern Annular Mode (SAM) [26].

Nevertheless, the literature generally lack an explicit study of wave period trends, given its importance to estimate the coupling of the ocean resource with the natural frequency of the device, that is, the resonance effect that should be found by the WEC to maximise the power absorption. In fact, the Cummins equation, which describes the motion of ships under the influence of incoming waves is used for the description of floating bodies in wave energy studies, but seeking the resonance by means suitable control systems instead of seeking the equilibrium [27,28]. Thus, the importance of wave period is crucial, mainly if we analyse the WEC's performance using adimensional ratios relative to the available power such as the Capture Width Ratio (CWR) described in Section 2.2.3. For instance, this aspect has been recently underlined by Fox et al. [29], who analysed Oscillating Water Column device (OWC) configurations in breakwaters, showing that these devices have a higher hydrodynamic efficiency in climates with low wave periods such as the Mediterranean.

The relative value of CWR as a performance indicator of the productivity of a given WEC is therefore more interesting to analyse the long-term evolution of wave energy than the usual trend analysis of the wave energy flux. A complete analysis of wave energy trends needs a further step to treat the historical variations of real wave energy production in terms of electricity production and the corresponding techno-economic assessment.

Two CWR estimation models were used here based on empirical studies: one for an OWC modelled in the wave tank of Florence [30], and the other for a patent based on a floating body that can be filled with water to change its inertial moment and consequently its natural frequency [31]. The discussion in Section 4 also explains the importance of the deviation from the resonance point in a qualitative manner, showing the influence of the identified wave period changes on the power matrices of floating bodies of different sizes.

The remainder of this paper is organised as follows: Section 2.1 presents the data and methodology for the study of wave trends; Section 2.2 describes the method to obtain the decadal changes in the percentage of wave period globally, the calibration technique via quantile matching, and empirical models of an OWC and a floating body; Section 3 introduces the corresponding results with the maps and behaviour of the two WECs' CWR; Section 4 discusses these results; and Section 5 presents the main conclusions and suggests future lines of research. Thus, the narrative logic is as follows: rough reanalysis data are used in the first global results for the identification of a relevant location according to wave period variation. Subsequently, a finer study based on calibration and real wave energy production for two different WECs was developed at these paradigmatic points.

2. Data and methodology

2.1. Data

2.1.1. ERA-20C

For data from the last century, the reanalysis ERA-20C of the ECMWF were used [32]. The observations assimilated are surface and mean sea level pressures from ISPDv3.2.6 and ICOADSv2.5.1, and surface marine winds from ICOADSv2.5.1., and the spatio-temporal evolution of background errors were produced a priori [33,34].

The temporal resolution of this model covers the period of 1900–2010 and his spatial resolution is approximately 125 km. ERA-20C was developed via IFS-Cy38r1, and a coupled Atmosphere/Land-surface/Ocean-waves model was used to assimilate surface observations. There are 91 levels in the vertical direction, the land-surface is distributed on four soil layers, and the ocean waves are distributed on 25 frequencies and 12 directions.

Monthly means were used for the analysis of trends of peak period, and for the particular analysis of energy production and capture width ratio at key locations three-hourly data is used, introducing the significant wave height for these cases. Finally, annual averages have been used to represent the trends of capture width given the usual annual character of energy production indexes.

According to the World Meteorological Organization, a 30-year period must be used for the analysis of climatologies [35]. Considering the years available in this dataset, the data from years 1981 to 2010 covers the last available 30-years period. Then, two additional non-overlapping 30-year periods have been defined going backwards from the most recent one, 1951–1980 and 1921–1950.

2.1.2. ERA5

The global trend analysis for the wave period was performed using rough ERA-20C data, but for locations of interest, where important historical and future wave period variations have been identified, ERA-20C was calibrated against ERA5 reanalysis [33], the most advanced reanalysis of the ECMWF. It covers the period from 1950 to the present, and thus, the calibration period was adopted between 1980–2009 (40 years). Produced by the Copernicus Climate Change Service at the ECMWF, this reanalysis presents 1-hourly temporal resolution and a spatial grid of 30 km for the atmosphere, and 80 km for ocean waves. It is therefore expected that this calibration procedure versus ERA5 will improve the ERA-20C historical data, given its good validations against wind and wave observations shown in the recent literature [16,36–41].

2.2. Methodology

2.2.1. Global changes

The median values of the peak wave period from ERA-20C were calculated at the global scale for the 30-year periods 1921–1950 (used as a reference) and the percent changes of the median period at every point with respect to this reference period were computed for the thirty-year periods 1951–1980 and 1981–2010. The use of the median in this computation leads to more robust results, because this quantity is less sensitive to outliers and the wave period distribution is not a normal distribution. The use of a 30-year period for the definitions of climatology is customary in climatological literature, and considers the recommendations of the World Meteorological Organization [35].

Thus, given 1921–1950, 1951–1980, and 1981–2010 time-intervals, the variation in percent of the median of the second period with respect to the first one for a parameter T is

$$\Delta T\% = 100 \times \frac{\tilde{P}_{1951-1980} - \tilde{P}_{1921-1950}}{\tilde{P}_{1921-1950}} \quad (1)$$

This percentage representation based on median has been applied in Fig. 2 for the variation of the second and third 30-year time-interval versus the first one.

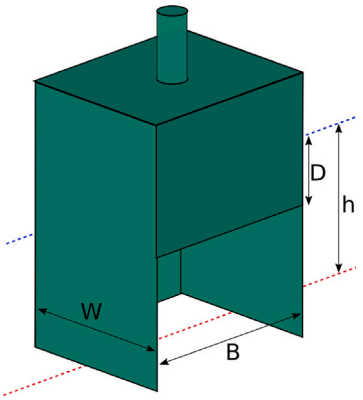

Fig. 1. Main geometrical parameters of an OWC according to its dimensions: chamber length B and width W, water draught D, and water depth h.

2.2.2. Calibration via quantile mapping

Quantile mapping was used for the calibration of the above mentioned reanalyses: ERA-20C versus ERA5 nearest gridpoint within the 1981–2010 period (40 years) selecting 3-hourly data for ERA5 in order to match ERA-20C time resolution (116800 cases analysed at a selected gridpoint). The authors have used this technique for wave energy potential studies over the past decades [14,15,17], mainly calibrating ERA-20C versus ERA-Interim [42], the previous reanalysis of the ECMWF.

This bias correction method based on the matching of the same quantile of two time series creating a transference function for each element of the series (from ERA-20C to ERA5 in our case) has different names in the literature: quantile mapping [43], probability mapping [44], statistical downscaling [45] and histogram equalisation [46]. The literature provides numerous examples of quantile mapping for temperature, precipitation, wind speed or other parameters [38,47–51]. Therefore, the calibration of the wave data can be considered a novelty previously introduced by these authors in the context of renewable marine energy capture.

2.2.3. Capture width ratio estimation model for OWC

The absorption width (B), length (W), draft (D), and the water depth (h) define the main geometrical parameters of an OWC according to the dimensions of its inferior cavity and the distances with respect to the water level (Fig. 1). For simplicity, the width and length are considered equal ($B = W$, square cavity base) in this study.

Table 1 shows the set of equations presented in [30] according to their experiments in the Florence wave tank for OWC devices. The first column shows the main input parameters with assignment of typical values and ranges. The definitions of each parameter can be found in the Nomenclature table. In the second column, the corresponding non-dimensional parameters are defined, and a list of numerical coefficients is included. Finally, the third column shows the new parameters $(a, b, c, d, f_1, f_2, f_3)$ as a function of the numerical coefficients empirically obtained in the laboratory experiments (P_i, Q_i). This set of equations has been recently been used to optimise the OWC width according to the arriving wavelength [37], which can be expressed as a function of the wave period for high intermediate or deep waters according to the dispersion relation, in which $\tanh(kh) \approx 1$ [52], $k = 2\pi/\lambda$, and g is the gravitational acceleration.

$$\lambda = \frac{g}{2\pi} T_p^2 = 1.56 T_p^2 \quad (2)$$

This final set of equations provides the main performance parameter of a wave energy converter, that is, the capture width ratio (CWR_{OWC}), defined and computed as follows:

$$\frac{f_1}{f_2 f_3 c} = CWR_{OWC} = \frac{P_{abs}}{P_{wave}} = \frac{P_{abs}}{WEF \cdot B} \quad (3)$$

Table 1
Main input, adimensional, and numerical parameters and the corresponding equations of the empirical OWC model to obtain its CWR.

Parameters	Adimensional par.	Empirical equations
H=3 m	$h_x = kh$	$a = \frac{P_3 h_x + P_4}{h_x^2 + Q_3 h_x + Q_4}$
λ=[50,150] m	$D_x = \frac{D}{Hcosh(k(h-D))cosh(kh)}$	$b = P_5 h_x^2 + P_6 h_x + P_7$
$k = 2\pi/\lambda$	$W_x = W/\lambda$	$c = P_8(h_x + P_9) + P_{10}$
$g = 9.8 m/s^2$	$K_x = \frac{KBW}{\rho_a^{1/2}}$	$d = P_{11} h_x^3 + P_{12} h_x^2 + P_{13} h_x + P_{14}$
$h = 20$ m		$f_1 = \frac{P_1(K_x - d) + P_2}{(K_x - d)^2 + Q_1(K_x - d) + Q_2}$
$K = 1.4$ Ns/m		$f_2 = \exp(aD_x)$
$\rho_a = 1.2$ kg/m^3		$f_3 = 1 + (W_x - W_{xopt})^2 b$
B = [7.5, 11.5] m		

where P_{abs} is the power absorbed by the OWC and P_{wave} is the energy of the wave flux (WEF) multiplied by the width of the OWC cavity, which is proportional to the square of the significant wave height and mean energy period.

$$WEF = \frac{\rho g^2}{64\pi} H_s^2 T_e = 0.49 H_s^2 T_e \ (\mathrm{kW/m}) \quad (4)$$

It should be noted that the mean period T_m was used for the computation of WEF in ECWMF reanalyses according to its parameter details [53], that is, mean wave period is actually energy period for ECWMF models and reanalyses for its approximation in deep waters for WEF.

On the other hand, the peak period T_p should be used for validation or implementation of the wave period on power matrices of different wave energy converters. Cahill et al. [54] defined a scale factor as wave period ratio for the correction of different definitions of wave period. Moreover, these empirical scale measurements were made in Irish sites such as AMETS (Atlantic Marine Energy Test Site) and Loop Head, near our selected gridpoint (Section 3.2). However, these scale corrections of wave period, obviously, are not relevant for relative increment in percent presented here, since a scale factor does not affect the slope of a regression. That is why the direct projections of T_m are used in Section 3.3.1.

2.2.4. Capture width ratio estimation for a floating body

For a second paradigmatic wave energy converter, a floating buoy of the same diameter as that used in the patent by Oigarden and Olsen was modelled in deep water [31] (O-FB). This power plant was achieved by designing the floating bodies to float awash and be partially filled with water, increasing or reducing the water mass within, thus allowing the natural frequency of the structure to be matched to the wave period, which is the key parameter in our study.

According to a previous empirical study, the wave power can be extracted in kW as a function of H_s and T_p [31,55]:

$$P_{abs} = 4.5 D_b^{2.4} H_s^{1.7} T_p^{-0.9} \quad (5)$$

where D_b denotes the diameter of the floating body. Therefore, the corresponding CWR can be obtained from Eq. (3) considering D_b as the withe of the device.

3. Results

3.1. 30-year variation of wave period

Fig. 2 shows the global variations in the percentage of peak wave period T_p using the entire ERA-20C period. In this plot, every three-decade period (1951–1980 and 1981–2010) is compared with the initial period (1921–1950) row by row to represent the transition of these changes during the 20th century in percent along with the wave period corresponding to 1921–1950.

The figure shows a generalised increase in the period for the Northern Hemisphere with larger values over specific areas, such as Newfoundland, Ireland and Japan in extratropical areas and increases in tropical Pacific areas. In some regions, such as the Indian Ocean, northern tropical Atlantic, or large areas of the Southern Hemisphere, some reductions in the period were also detected, even though they were weaker than the overall increase. If the spatial average of the percentage change is computed, it is weak but positive during the 1951–1980 period (0.2%), but an order of magnitude larger (2%) during 1981–2010. These results obtained using ERA5 data, are in some cases consistent with the findings of other studies particularly over some areas of the Southern Hemisphere (Pacific) but diverge in other regions, such as the Northern Atlantic [23,56]. At the regional scale, there are some recent similar findings regarding the energy period over the Mediterranean [57] or the Black Sea [58].

3.2. Wave climate change in Ireland

Ireland was selected for the regional analysis for two reasons: first, the strong wave period changes identified in the previous global analysis, and second, because it possesses one of the richest wave energy climates in the world. According to the Foras na Mara Marine Institute (https://www.marine.ie), wave energy resources potentially available to Ireland could meet 75% of country's electricity requirements.

Fig. 3 shows the evolution of H_s, T_p and WEF in the most energetic western sea area of Ireland. Based on the figure panel, a particular analysis grid point (star symbol) was selected near the Bay of Galway [−11°, 53°] because of its relevance as a transition zone through the three 30-year periods (rows: 1921–1950, 1951–1980, 1981–2010). The increment in the values was clear for the wave height and period and the corresponding value of WEF, which reached an increment of almost 40% according to the isoline in the last historical period compared to the nearness of the 25% increment isoline in the second 1951–1980 period. The cause of these strong increments of WEF is the corresponding strong increment of H_s (around 16% in the last period), with a lower but relevant increment of wave period.

In addition to high resource potential, Galway is also well known as a scale wave energy test site [59]. Furthermore, the ECMWF reanalyses used here have been validated against buoys of the Foras na Mara Marine Institute (https://www.marine.ie) in previous studies for this area and other locations in Ireland [14,60]. These aspects make [−11°, 53°] and the sub-area near Galway a relevant grid point for our posterior study on the historical behaviour of the OWC's and O-FBs' performance.

Fig. 4(a) shows the colour map of the bathymetry around the Galway Bay from EMODNET [61], where our analysis point was located with a transect line connecting the coast. Below, Fig. 4(b), the vertical profile of the transect shows a depth of approximately 150 m at a distance of 100 km from the coast. The depth ensures a deep-water approximation for the dispersion relation while establishing a relatively low anchoring depth, and the distance for the coast is also short and reasonable for operation and maintenance issues.

3.3. CWR reduction of WECs: the paradigmatic case at the selected point

Calibrated data of ERA-20C versus ERA5 were used to study the trend of wave period and CWR of the two devices at the selected gridpoint [−11°, 53°]. Given that the energy production is almost always evaluated annually, annual averages of wave period and CWR have been computed after the calibration in order to apply the trend analysis.

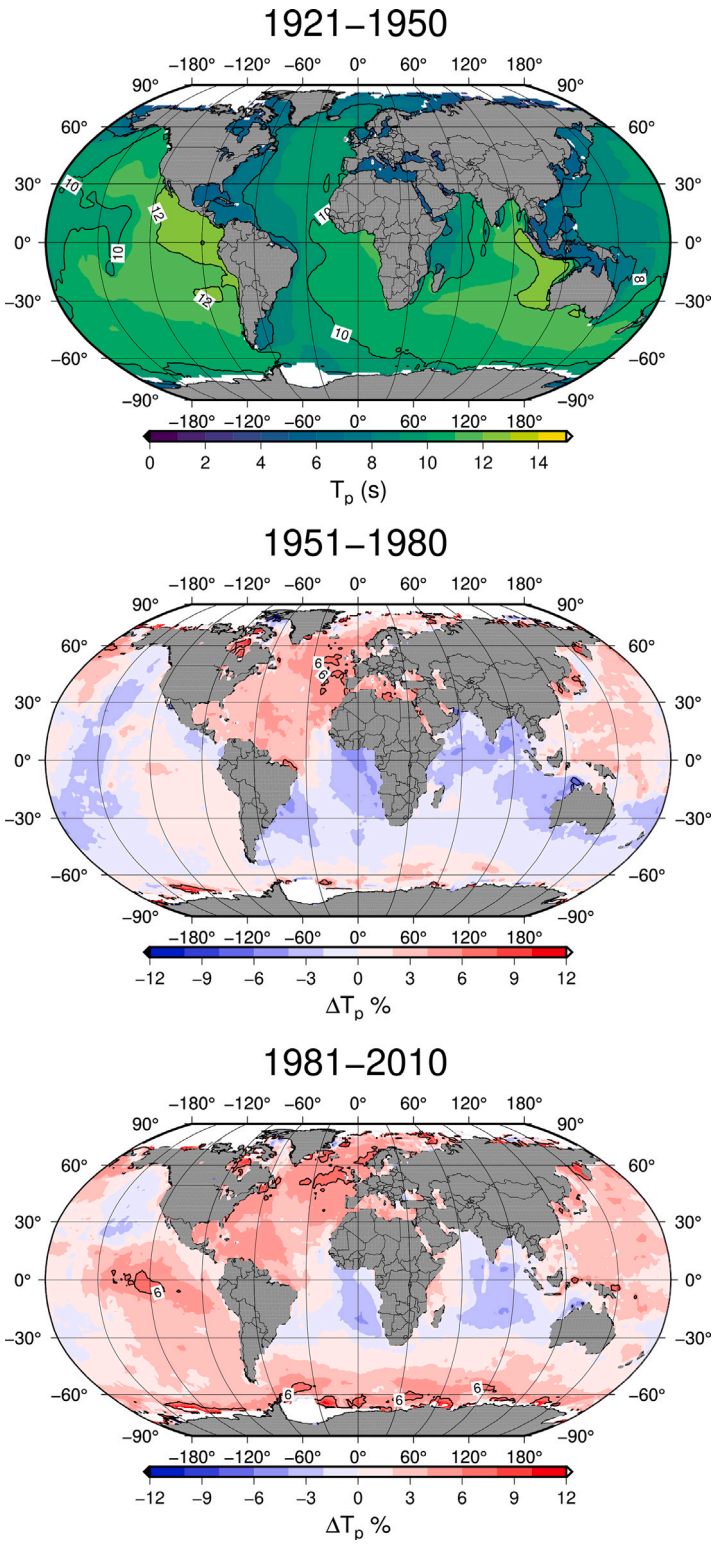

Fig. 2. Global median of wave peak period (s) in the Northern and Southern hemispheres during the 1921–1950 period (top) and percent change with respect to 1921–1950 during the time-intervals 1951–1980 (middle) and 1981–2010 (bottom).

3.3.1. *Wave period evolution*

The selected site showed a clear and significant increase in T_m during the 110 years starting in 1900 (Fig. 5). The fitting of the slope line and its shaded area to represent the confidence interval at 95% was computed using the Theil–Sen method [62] for annual average values of the wave period (110 cases), and subsequently, the corresponding $CWRs$. Annual $\overline{T_m}$ and both annual $\overline{CWRs}$ are therefore respectively represented in Fig. 5, Fig. 6 and Fig. 7.

The confidence intervals at a 95% of the slope given by the Theil–Sen method were [0.57, 0.67] s per century, indicating a significant result. A considerable increment of 0.6 s from 7.8 s establishes a relative increment of approximately 8%.

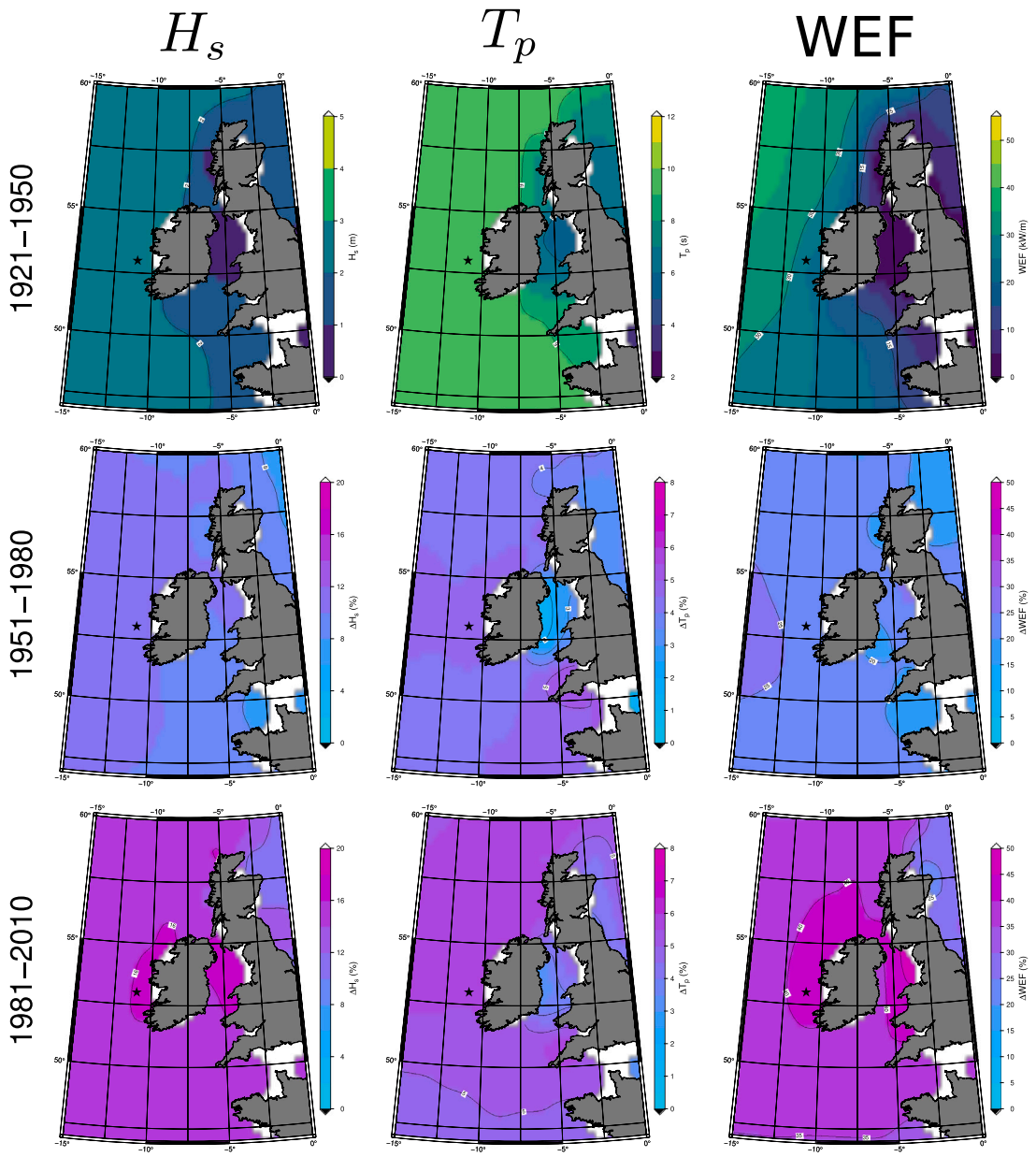

Fig. 3. Significant wave height (first column), peak period (second column), and wave energy flux (third column) changes during the three 30-year periods (rows) in Ireland. The grid point [−11°, 53°] was selected and marked because if its relevant position in the historical transition zone.

3.3.2. *CWR evolution of OWC*

The selected grid point also showed a significant increment at the 95% confidence level of CWR in Fig. 6 for the OWC model. The typical initial values of Table 1 were not in the optimum working point in the sea conditions of 1900, but the approximation towards this optimum power during the evolution of the 20th century shows a clear increase in CWR.

The 95% confidence intervals of the CWR slope given by the Theil–Sen method were [0.073,0.082] per century, indicating a significant result. In relative terms, this represents an increment of approximately $\approx 20\%$ for CWR over the century, and means an even higher increment of annual or decadal power production given the increment of the average WEF.

3.3.3. *CWR evolution of O-FB*

Fig. 7 shows a very significant reduction in CWR for the O-FB model for the confidence intervals computed by the Theil–Sen technique [62] and Eq. (5). The typical working parameters described in [31,55] were used to establish working conditions between 1900 and 2010.

The confidence intervals at a 95% of the CWR slope were [−0.101, −0.0870] per century, showing a significant result. The initial $CWR = 0.50$ decreased to approximately 0.40 with a loss of $\approx 20\%$ in a century, that is, a negative slope of approximately −2%/decade.

4. Discussion

In order to discuss these results about the floating body O-FB in Fig. 7, based on a simple development of Eq. (5), the corresponding equation for the capture width ratio of the floating body (CWR_{fb}) is proportional to

$$CWR_{fb} \propto H_s^{-0.3} T_p^{-1.9}. \tag{6}$$

This indicates a very low dependence on H_s and a high dependence on T_p, the increment of which can significantly reduce the performance according to CWR, as detected in many areas of the world.

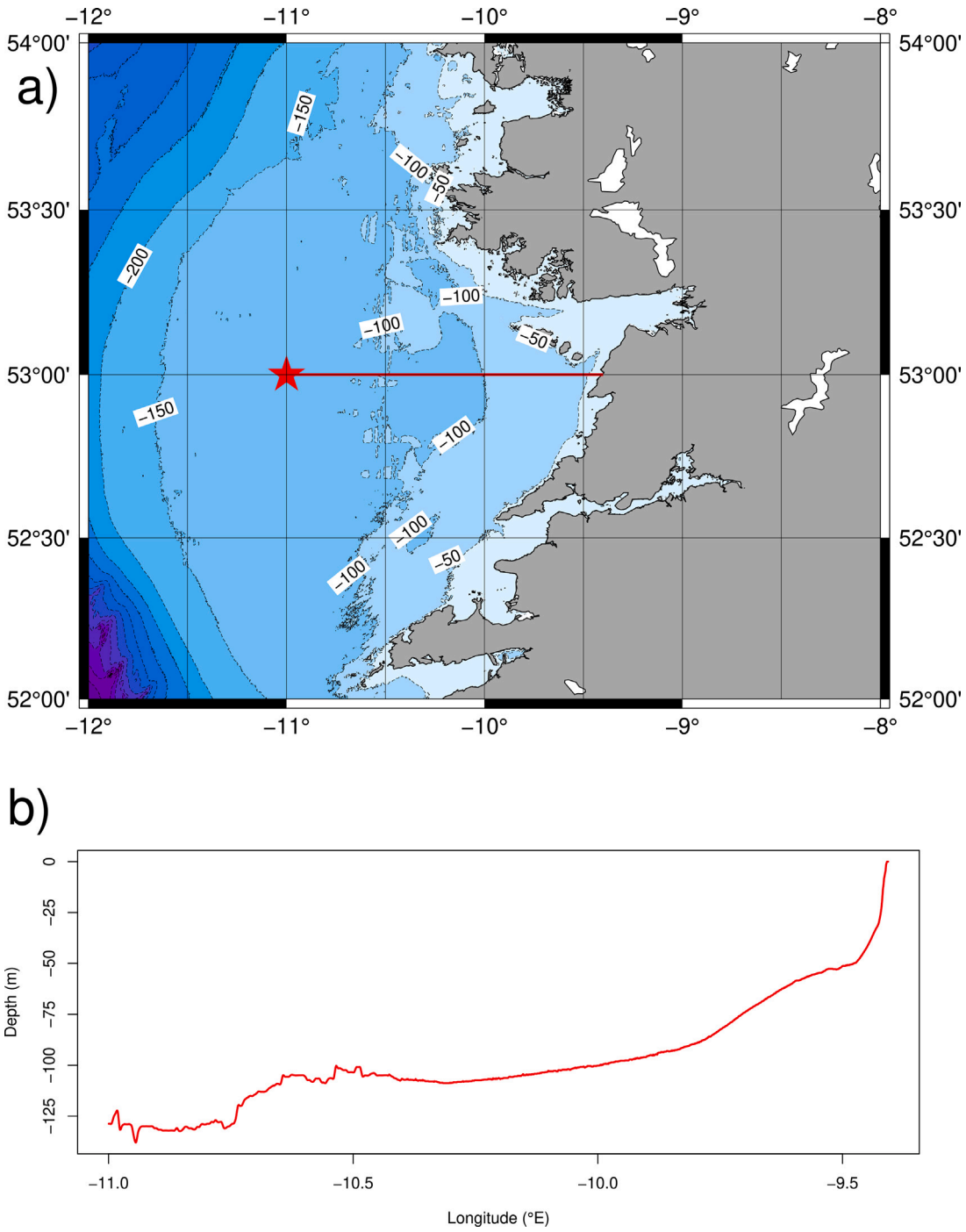

Fig. 4. Bathimetry map (a) and transect profile (b) from the Irish coast to the analysis site [−11°, 53°] along the latitude 53°N.

Assuming the error theory for the wave period as a single variable and calculating the corresponding derivatives for the relative error $\Delta CWR_{fb,r}$

$$\Delta CWR_{fb,r} = \frac{\Delta CWR_{fb}}{CWR_{fb}} = \\ = \frac{\partial CWR_{fb}}{\partial T_p}\frac{\Delta T_p}{CWR_{fb}} + \frac{\partial CWR_{fb}}{\partial H_s}\frac{\Delta H_s}{CWR_{fb}} = -1.9\Delta T_{p,r} - 0.3\Delta H_{s,r}. \quad (7)$$

This indicates that the value of the relative increment of the wave period corresponds to a reduction of approximately double the performance and that the wave height variation does not affect it. In our case, an increment of approximately 10% for the wave period produced a reduction of approximately 20% in the O-FB performance according to its CWR.

An analogous paradigmatic example can be described for other simple floating bodies such as the WaveBot devices shown in Figs. 8(a) and 8(c), which have been modelled using the open-source boundary element method (BEM) solver NEMOH [63]. Compliant with the premise above, it is demonstrated that the variation in the wave period remarkably affects the power production of the point absorbers [64], as the production shifts away from the frequency of maximum absorption, as shown in Figs. 8(a) and 8(c).

The geometrical properties of the point absorbers and the design of the Power Take-Off (PTO) system define the frequency of maximum power absorption. With the development of the industry, larger devices

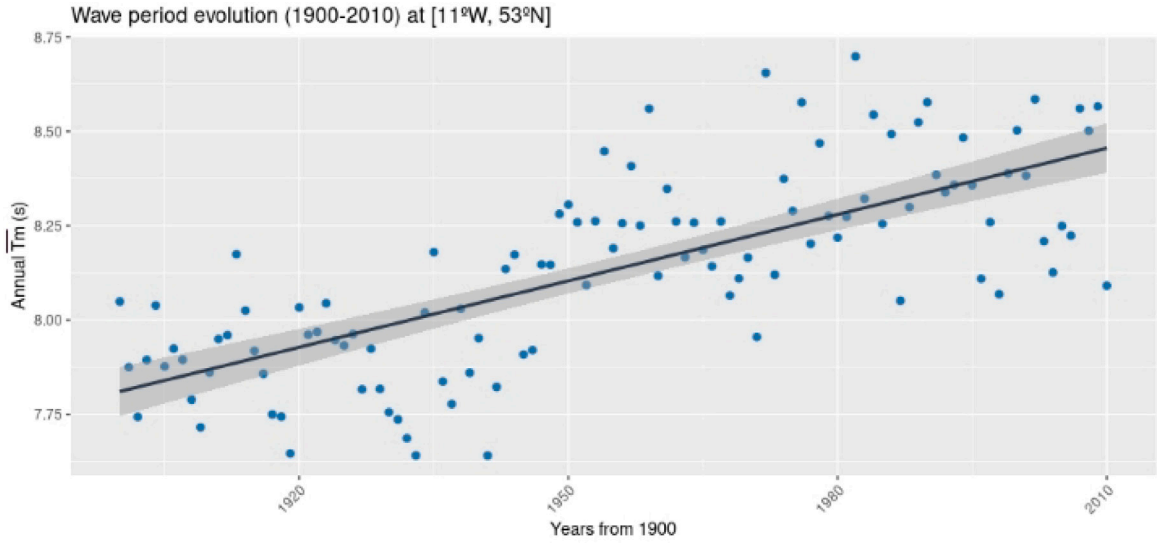

Fig. 5. Increment of wave period (annual average, $\overline{T_m}$) from 1900 to 2010 at the selected grid point at [−11°, 53°]. The shaded area around the slope indicates the confidence interval at a 95% confidence level.

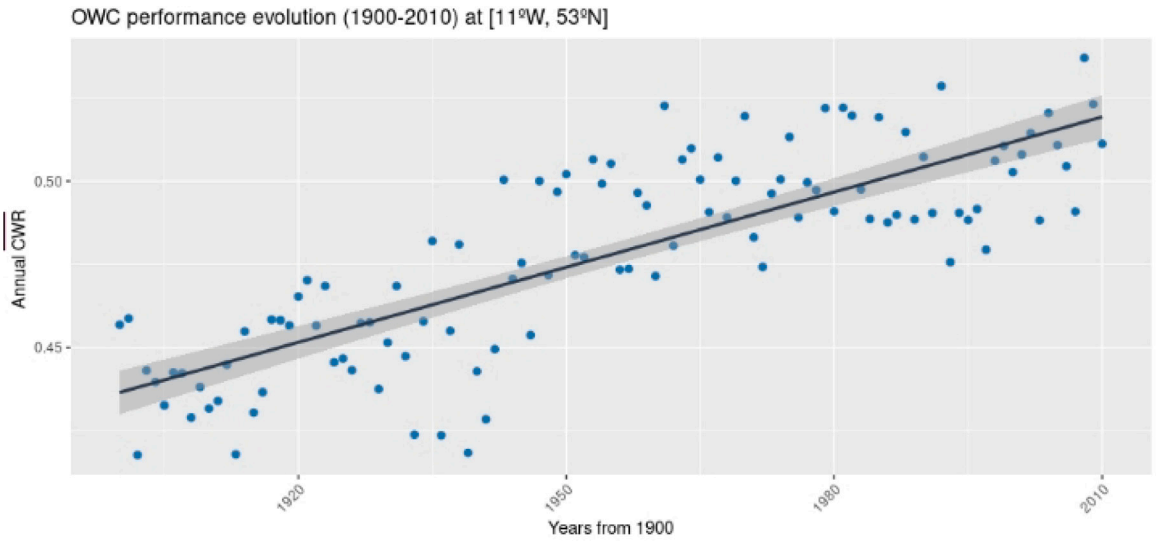

Fig. 6. Increment of capture width ratio performance (annual average, $\overline{CWR}$) of the OWC device from 1900 to 2010 for the selected grid point at [−11°, 53°]. The shaded area around the slope indicates the confidence interval at a 95% confidence level.

will be designed and, as a result, the maximum absorption will shift to higher wave periods. This could be beneficial in terms of the wave period tendency.

Similarly, Fig. 9 shows how the optimum working point of the OWC model suffers an important displacement due to different wave periods (T_m 7.5 s on the left, and 8.5 s on the right) around the values obtained in the historical development of the wave period for the selected site. Thus, a chamber length $B \approx 14$ m, such as the one adopted in our case and a significantly lower damping coefficient, would produce the maximum instantaneous performance according to CWR, closer to the conditions of the last 1981–2010 historical period. This analysis considers the constant values of the chamber dimensions and damping during these historical trends, offering a qualitative physical explanation for the results obtained in Fig. 6.

According to these qualitative explanations of the obtained results, the variations observed in Ireland should be similar to other regions of the world according to the historical evolution shown in Fig. 2. Although they do not show as much wave energy potential as Ireland, the increments and reductions of the wave period should be underlined in these regions:

- Increment in the Caribbean, Central America, Papua, or Polynesia,
- Reduction in Gulf of Guinea, Indian Ocean, and Gulf of Alaska.

Nevertheless, it should be also noted that regions with high wave exploitability such as Chile and South of Australia [65] does not show strong historical wave period variations, and this fact can be interesting for future development of wave energy plants considering other criteria apart from average wave power such as its variability.

Recent studies using other reanalysis data and dynamic downscaling for waves corroborate these strong trends for other wave energy production indices [66], such as wind data of the Japanese JRA-55 model with spatial and temporal resolutions of 60 km and 6 h [67], respectively, forcing the numerical wave model SWAN (Simulating Waves Nearshore) Cycle III version 41.31. According to them, the selection period for wave energy assessment can lead to an over/underestimation of approximately 25% of theoretical wave energy flux. Therefore, the identified patterns are even stronger than those in our study, but they do not implement real devices and the consequent wave energy production.

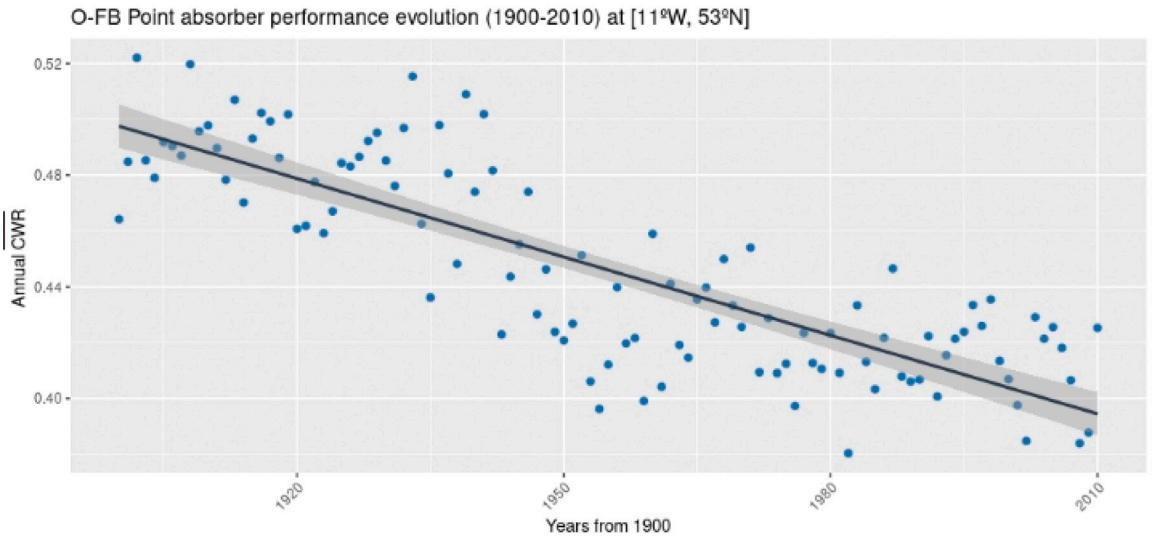

Fig. 7. Reduction of CWR performance (annual average, $\overline{CWR}$) for the O-FB device from 1900 to 2010 for the selected grid point at [11°W, 53°N]. The shaded area around the slope indicates the confidence interval at a 95% confidence level.

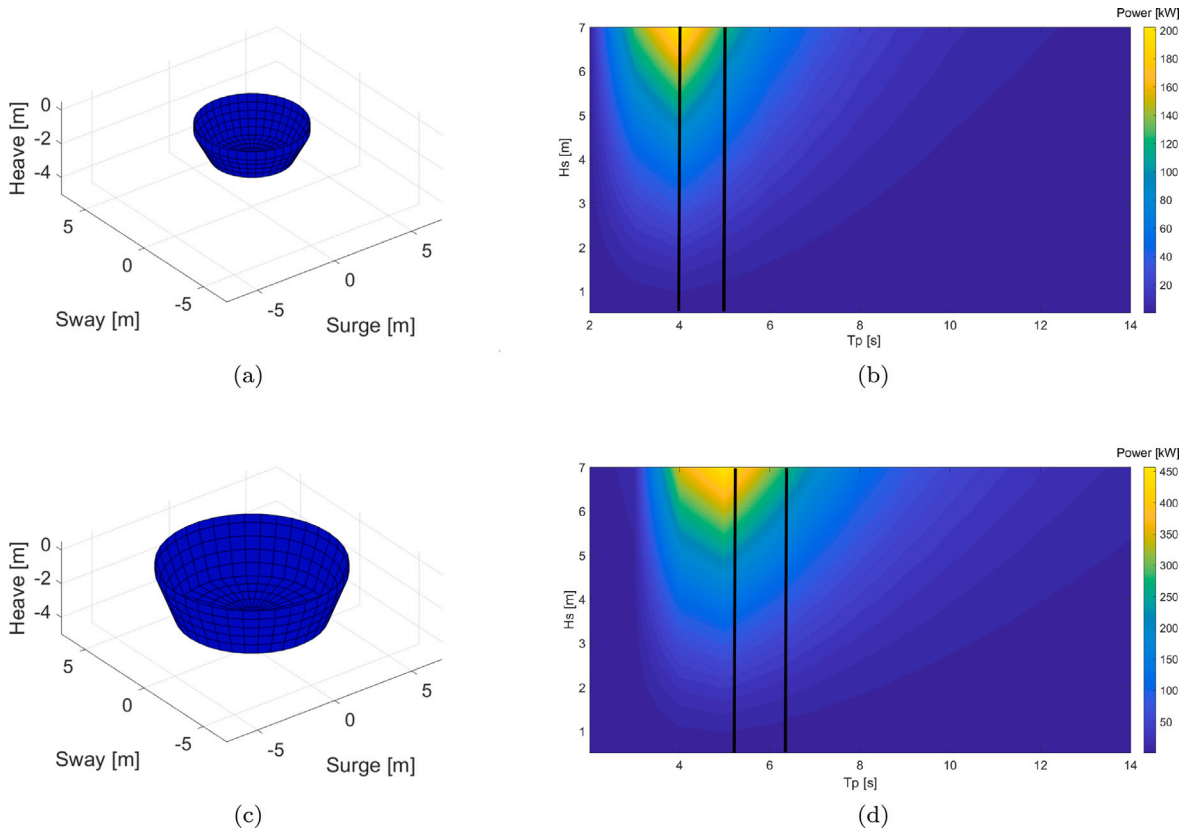

Fig. 8. (a) Mesh for the NEMOH based hydrodynamic analysis of a 6 m diameter WaveBot point absorber. (b) Power matrix of a 6 m diameter WaveBot point absorber. (c) Mesh for the NEMOH based hydrodynamic analysis of a 10 m diameter WaveBot point absorber. (b) Power matrix of a 10 m diameter WaveBot point absorber.

The authors are not aware of similar global-scale studies that discuss this effect based on reanalysis data during the last 70 years, as was done in this study. However, there are some studies which have used the results from global climate models from the CMIP5 dataset, RCP-8.5 scenario [23,56] by the end of the 21st century. As such, we cannot expect the results to be directly comparable, because the current forcing is still weaker than that corresponding to that scenario. However, in some cases, the changes in the period detected in this study were consistent with those reported in those studies. This is the case for the tropical Pacific, in which the changes detected are consistent with those expected from changes in Hadley circulation [56]. Changes in the period in the Southern Hemisphere are consistent with increased storm-track activity in the southernmost latitudes [68] and an increase in swell propagated northward [56]. However, the sign of the changes in wave period identified in this study (Fig. 2), calculated using wave data from ERA-20C calibrated by means of ERA5 data are not fully consistent with results from climate models used in other studies [23,56] over the North Atlantic and Pacific. At least three possible explanations

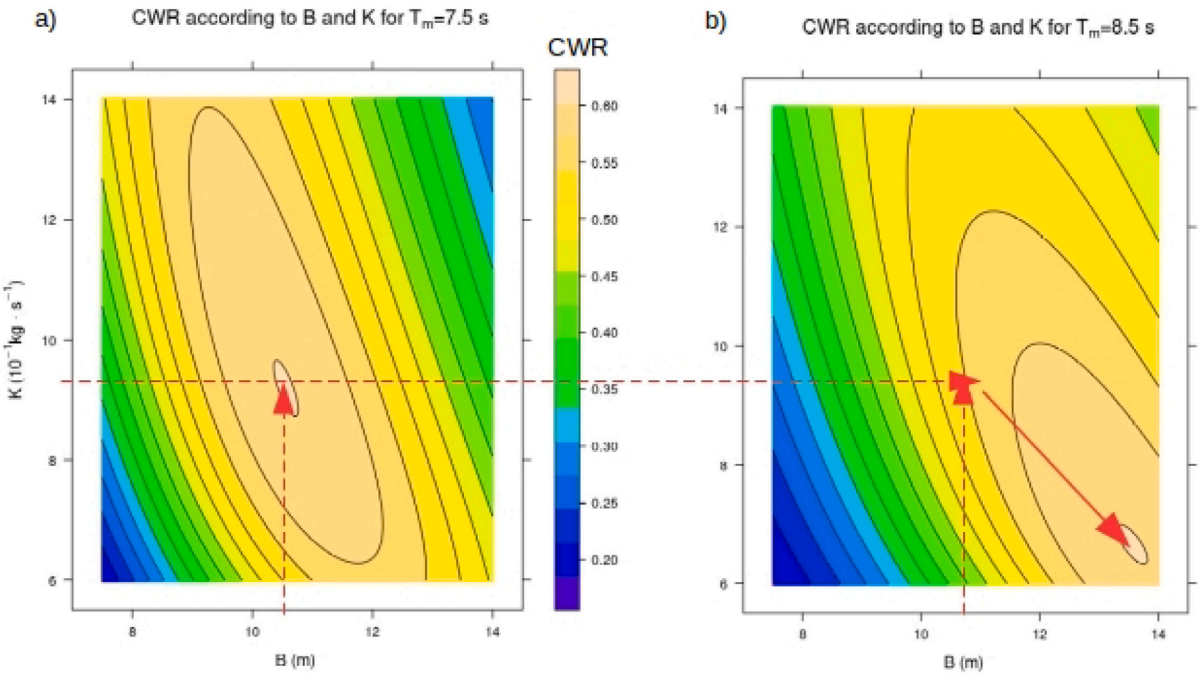

Fig. 9. Displacement of the optimum instantaneous CWR for the OWC model according to the approximate values of wave period analysed at the relevant location, and typical values of B ≈ 11 m, and $K \approx 0.9$ kg s^{-1}: (a) CWR matrix versus K and B for a $T_m = 7.5$ s ; (b) CWR matrix versus K and B for a $T_m = 8.5$ s.

exist for this discrepancy: First, one explanation could be that some of the variability identified in this study is affected in different regions by decadal-scale variability such as the one induced by the AMO or the PDO [69] on the storm tracks in addition to the changes that are expected due to global warming, which is still weak. In this regard, the study period would still appear in the realm of interannual or decadal-scale noise. However, the changes identified in this study (Fig. 2) showed a large degree of spatial consistency throughout the periods of 1951–1980 and 1981–2010, with changes that intensified over time in the same regions. This indicates that the results are robust to some extent. The only exception to this is that there are still some spurious trends in the reanalysis data due to time-varying data coverage [70]. In any case, it must also be considered that a limited set of climate models using the RCP8.5 scenario are not able to reflect the full variability of the wave period at the global scale.

However, some studies at smaller scales give some confidence to the findings presented in this study. An analysis of the trends of wave properties (significant height, energy period and wave power) over the Mediterranean from 1979 to 2018 [57] found an increasing trend over the area, as also shown in Fig. 2 of this paper. Similarly, a dipolar structure in the decadal characteristics of the wave power between 1979–1988 to 2006–2015 over the Black Sea, with negative(positive) changes of wave power in the Western(Eastern) basis of the Black Sea has also been identified [58], consistent with the results shown in our Fig. 2.

On the other hand, a study focused in the analysis of wave data from ERA Interim around Southern Italy [71] from 1979 to 2017 shows a positive trend for period over southern Italy. On the other hand, the study of the trends of wave period under an RCP8.5 forcing using an ensemble of seven CMIP5 models shows a downward trend over that area for the period 2006–2100.

Thus, the divergence between the trends calculated during the last decades and the changes due to greenhouse forcing is still an open question which will require further research with alternative datasets and studies focusing on these issues. However, that is outside of the scope of this paper, which is focused on the response of an energy converter to changes in the period of the waves that can be expected in the future.

5. Conclusions

Strong variations in wave energy converter performance of approximately ± 20% have been found in models of wave period changes in the 20th century. This requires necessary a long-term perspective for initial dimensioning and damping control strategies. The performance measured as an adimensional capture width ratio is highly sensitive to wave period variations, even losing its optimum value for regions such as Ireland where the long-term historical wave energy potential is being incremented in absolute terms of WEF.

Hence, the selection of this location with strong historical WEF increments is not technically casual, because the ratio defined in CWR increments its denominator and reduces its numerator due to the displacement of the resonant point. This behaviour has been analytically demonstrated by the particular case of the O-FB floating device in Eq. (7), in which the dependence on wave height of CWR is negligible, and a strong dependence on wave period is shown. That is why the selected gridpoint in Ireland is considered a paradigmatic case, and a similar error estimation based on differential analysis can offer analogous relationships for other WECs.

The hypotheses of this study established a constant damping coefficient and chamber or floating body dimension during the analysis period, without considering long-term control and regulation systems, the possibility of varying the width of the chamber, or the size of the floating body to adapt its moment of inertia to the natural frequency or the optimum wave period. This work demonstrates that these structural variations could be interesting for future research.

Furthermore, the implementation of CMIP6 future simulations until 2100 applying dynamic down-scaling to obtain future wave climate data can extend these past results towards the future in SSP socioeconomic scenarios, expecting future relevant performance variations where wave period changes are identified, such as in the recent case of CMIP5 using RCP scenarios [72].

Declaration of competing interest

The authors declare that they have no known competing financial interests or personal relationships that could have appeared to influence the work reported in this paper.

Data availability

Data will be made available on request.

Acknowledgements

This study is part of project PID2020-116153RB-I00 funded by Ministerio de Ciencia e Innovación/Agencia Estatal de Investigación, Spain MCIN/AEI/ 10.13039/501100011033. The authors acknowledge the funding of the research groups by the University of the Basque Country, Spain (UPV/EHU, GIU20/08).

References

[1] IRENA. Renewable energy: A key climate solution. Tech. rep., International Renewable Energy Agency; 2017.
[2] Jacobson MZ, Delucchi MA, Bauer ZA, Goodman SC, Chapman WE, Cameron MA, et al. 100% Clean and renewable wind, water, and sunlight all-sector energy roadmaps for 139 countries of the world. Joule 2017;1:108–21. http://dx.doi.org/10.1016/j.joule.2017.07.005.
[3] Weiss CV, Guanche R, Ondiviela B, Castellanos OF, Juanes J. Marine renewable energy potential: A global perspective for offshore wind and wave exploitation. Energy Convers Manage 2018;177:43–54. http://dx.doi.org/10.1016/j.enconman.2018.09.059.
[4] Clemente D, Rosa-Santos P, Taveira-Pinto F. On the potential synergies and applications of wave energy converters: A review. Renew Sustain Energy Rev 2021;135:110162. http://dx.doi.org/10.1016/j.rser.2020.110162.
[5] Abanades J, Greaves D, Iglesias G. Coastal defence through wave farms. Coast Eng 2014;91:299–307. http://dx.doi.org/10.1016/j.coastaleng.2014.06.009.
[6] Pérez-Collazo C, Greaves D, Iglesias G. A review of combined wave and offshore wind energy. Renew Sustain Energy Rev 2015;42:141–53. http://dx.doi.org/10.1016/j.rser.2014.09.032.
[7] Reguero BG, Losada IJ, Méndez FJ. A recent increase in global wave power as a consequence of oceanic warming. Nature Commun 2019;10(1):1–14. http://dx.doi.org/10.1038/s41467-018-08066-0.
[8] Reguero B, Losada I, Méndez F. A global wave power resource and its seasonal, interannual and long-term variability. Appl Energy 2015;148:366–80. http://dx.doi.org/10.1016/j.apenergy.2015.03.114.
[9] Lobeto H, Menendez M, Losada IJ. Future behavior of wind wave extremes due to climate change. Sci Rep 2021;11(1):1–12. http://dx.doi.org/10.1038/s41598-021-86524-4.
[10] Young I, Zieger S, Babanin AV. Global trends in wind speed and wave height. Science 2011;332(6028):451–5. http://dx.doi.org/10.1126/science.1197219.
[11] Bouws E, Jannink D, Komen G. The increasing wave height in the North Atlantic Ocean. Bull Am Meteorol Soc 1996;77(10):2275–7. http://dx.doi.org/10.1175/1520-0477(1996)077<2275:TIWHIT>2.0.CO;2.
[12] Gulev SK, Grigorieva V. Variability of the winter wind waves and swell in the North Atlantic and North Pacific as revealed by the voluntary observing ship data. J Clim 2006;19(21):5667–85. http://dx.doi.org/10.1175/JCLI3936.1.
[13] Odériz I, Mori N, Shimura T, Webb A, Silva R, Mortlock T. Transitional wave climate regions on continental and polar coasts in a warming world. Nature Clim Change 2022;2383–402. http://dx.doi.org/10.1038/s41558-022-01389-3.
[14] Penalba M, Ulazia A, Ibarra-berastegui G, Ringwood J, Sáenz J. Wave energy resource variation off the west coast of Ireland and its impact on realistic wave energy converters' power absorption. Appl Energy 2018;224(2018):205–19. http://dx.doi.org/10.1016/j.apenergy.2018.04.121.
[15] Ulazia A, Penalba M, Rabanal A, Ibarra-Berastegi G, Ringwood J, Sáenz J. Historical evolution of the wave resource and energy production off the Chilean coast over the 20th century. Energies 2018;11(9):2289. http://dx.doi.org/10.3390/en11092289.
[16] Penalba M, Ulazia A, Sáenz J, Ringwood JV. Impact of long-term resource variations on wave energy farms: The Icelandic case. Energy 2020;192:116609. http://dx.doi.org/10.1016/j.energy.2019.116609.
[17] Ulazia A, Penalba M, Ibarra-Berastegi G, Saenz J. Wave energy trends over the Bay of Biscay and the consequences for wave energy converters. Energy 2017;141(C):624–34. http://dx.doi.org/10.1016/j.energy.2017.09.099.
[18] Patra A, Bhaskaran PK. Temporal variability in wind–wave climate and its validation with ESSO-NIOT wave atlas for the head Bay of Bengal. Clim Dynam 2016;1–18. http://dx.doi.org/10.1007/s00382-016-3385-z.
[19] Camus P, Losada IJ, Izaguirre C, Espejo A, Menéndez M, Pérez J. Statistical wave climate projections for coastal impact assessments. Earth's Future 2017;5:918–33. http://dx.doi.org/10.1002/2017EF000609.
[20] Caires S, Sterl A, Gommenginger C. Global ocean mean wave period data: Validation and description. J Geophys Res: Oceans 2005;110(C02003). http://dx.doi.org/10.1029/2004JC002631.
[21] Mackay E, Retzler C, Challenor P, Gommenginger C. A parametric model for ocean wave period from Ku band altimeter data. J Geophys Res: Oceans 2008;113(C3). http://dx.doi.org/10.1029/2007JC004438.
[22] Gommenginger C, Srokosz M, Challenor P, Cotton P. Measuring ocean wave period with satellite altimeters: A simple empirical model. Geophys Res Lett 2003;30(22). http://dx.doi.org/10.1029/2003GL017743.
[23] Patra A, Min S-K, Son S-W, Yeh S-W. Hemispheric asymmetry in future wave power changes: Seasonality and physical mechanisms. J Geophys Res: Oceans 2021;126(12):e2021JC017687. http://dx.doi.org/10.1029/2021JC017687.
[24] Bernardino M, Goncalves M, Guedes Soares C. Marine climate projections toward the end of the twenty-first century in the north atlantic. J Offshore Mech Arct Eng 2021;143(6):1–34. http://dx.doi.org/10.1115/1.4050698.
[25] Gao H, Liang B, Shao Z. A global climate analysis of wave parameters with a focus on wave period from 1979 to 2018. Appl Ocean Res 2021;111:102652. http://dx.doi.org/10.1016/j.apor.2021.102652.
[26] Ramos MS, Farina L, Faria SH, Li C. Relationships between large-scale climate modes and the South Atlantic Ocean wave climate. Prog Oceanogr 2021;197:102660. http://dx.doi.org/10.1016/j.pocean.2021.102660.
[27] Cummins W, Iiuhl W, Uinm A. The impulse response function and ship motions. Tech. rep., Citeseer; 1962.
[28] Falcão AFdO. Wave energy utilization: A review of the technologies. Renew Sustain Energy Rev 2010;14(3):899–918. http://dx.doi.org/10.1016/j.rser.2009.11.003.
[29] Fox BN, Gomes RP, Gato LM. Analysis of oscillating-water-column wave energy converter configurations for integration into caisson breakwaters. Appl Energy 2021;295:117023. http://dx.doi.org/10.1016/j.apenergy.2021.117023.
[30] Simonetti I, Cappietti L, Oumeraci H. An empirical model as a supporting tool to optimize the main design parameters of a stationary oscillating water column wave energy converter. Appl Energy 2018;231:1205–15. http://dx.doi.org/10.1016/j.apenergy.2018.09.100.
[31] Oigarden H, Olsen F. Wave power station, US Patent US7585131B2. 2009, URL https://patents.google.com/patent/US7585131B2/en.
[32] Poli P, Hersbach H, Dee DP, Berrisford P, Simmons AJ, Vitart F, et al. ERA-20C: An atmospheric reanalysis of the twentieth century. J Clim 2016;29:4083–97. http://dx.doi.org/10.1175/JCLI-D-15-0556.1.
[33] Hersbach H, Peubey C, Simmons A, Berrisford P, Poli P, Dee D. ERA-20CM: a twentieth-century atmospheric model ensemble. Q J R Meteorol Soc 2015;141(691):2350–75. http://dx.doi.org/10.1002/qj.2528.
[34] Poli P, Hersbach H, Tan D, Dee D, Thepaut J-N, Simmons A, et al. The data assimilation system and initial performance evaluation of the ECMWF pilot reanalysis of the 20th-century assimilating surface observations only (ERA-20C). European Centre for Medium Range Weather Forecasts; 2013.
[35] World Meteorological Organization. WMO guidelines on the calculation of climate normals. Tech. rep. WMO-no. 1203, Geneva, Switzerland: World Meteorological Organization; 2017, p. 18.
[36] Olauson J. ERA5: The new champion of wind power modelling? Renew Energy 2018;126:322–31. http://dx.doi.org/10.1016/j.renene.2018.03.056.
[37] Ulazia A, Esnaola G, Serras P, Penalba M. On the impact of long-term wave trends on the geometry optimisation of oscillating water column wave energy converters. Energy 2020;206:118146. http://dx.doi.org/10.1016/j.energy.2020.118146.
[38] Carreno-Madinabeitia S, Ibarra-Berastegi G, Sáenz J, Ulazia A. Long-term changes in offshore wind power density and wind turbine capacity factor in the Iberian Peninsula (1900–2010). Energy 2021;226:120364. http://dx.doi.org/10.1016/j.energy.2021.120364.
[39] Bruno MF, Molfetta MG, Totaro V, Mossa M. Performance assessment of ERA5 wave data in a swell dominated region. J Mar Sci Eng 2020;8(3):214. http://dx.doi.org/10.3390/jmse8030214.
[40] Rusu L, Rusu E. Evaluation of the worldwide wave energy distribution based on ERA5 data and altimeter measurements. Energies 2021;14(2):394. http://dx.doi.org/10.3390/en14020394.
[41] Shi H, Cao X, Li Q, Li D, Sun J, You Z, et al. Evaluating the accuracy of ERA5 wave reanalysis in the water around China. J Ocean Univ China 2021;20(1):1–9. http://dx.doi.org/10.1007/s11802-021-4496-7.
[42] Dee DP, Uppala SM, Simmons AJ, Berrisford P, Poli P, Kobayashi S, et al. The ERA-Interim reanalysis: Configuration and performance of the data assimilation system. Q J R Meteorol Soc 2011;137(656):553–97. http://dx.doi.org/10.1002/qj.828.
[43] Sun F, Roderick ML, Lim WH, Farquhar GD. Hydroclimatic projections for the Murray-Darling Basin based on an ensemble derived from Intergovernmental Panel on Climate Change AR4 climate models. Water Resour Res 2011;47(12). http://dx.doi.org/10.1029/2010WR009829.
[44] Block P, Souza Filho F, Sun L, Kwon H-H. A streamflow forecasting framework using multiple climate and hydrological models. J Am Water Resour Assoc 2009;45(4):828–43. http://dx.doi.org/10.1111/j.1752-1688.2009.00327.x, cited By 45.
[45] Piani C, Haerter JO, Coppola E. Statistical bias correction for daily precipitation in regional climate models over Europe. Theor Appl Climatol 2010;99(1):187–92. http://dx.doi.org/10.1007/s00704-009-0134-9.
[46] Rojas R, Feyen L, Dosio A, Bavera D. Improving pan-European hydrological simulation of extreme events through statistical bias correction of RCM-driven climate simulations. Hydrol Earth Syst Sci 2011;15(8):2599–620. http://dx.doi.org/10.5194/hess-15-2599-2011, cited By 45.

[47] Teutschbein C, Seibert J. Bias correction of regional climate model simulations for hydrological climate-change impact studies: Review and evaluation of different methods. J Hydrol 2012;456:12–29. http://dx.doi.org/10.1016/j.jhydrol.2012.05.052.

[48] Watanabe S, Kanae S, Seto S, Yeh PJ-F, Hirabayashi Y, Oki T. Intercomparison of bias-correction methods for monthly temperature and precipitation simulated by multiple climate models. J Geophys Res: Atmos 2012;117(D23). http://dx.doi.org/10.1029/2012JD018192.

[49] Bett PE, Thornton HE, Clark RT. Using the Twentieth Century Reanalysis to assess climate variability for the European wind industry. Theor Appl Climatol 2015. http://dx.doi.org/10.1007/s00704-015-1591-y.

[50] Li D, Feng J, Xu Z, Yin B, Shi H, Qi J. Statistical bias correction for simulated wind speeds over CORDEX-East Asia. Earth Space Sci 2019;6(2):200–11. http://dx.doi.org/10.1029/2018EA000493.

[51] Whan K, Zscheischler J, Jordan AI, Ziegel JF. Novel multivariate quantile mapping methods for ensemble post-processing of medium-range forecasts. Weather Clim Extrem 2021;32:100310. http://dx.doi.org/10.1016/j.wace.2021.100310.

[52] Sundar V. Ocean wave mechanics: Applications in marine structures. John Wiley & Sons; 2017.

[53] Details Parameters. ECMWF. 2022, https://apps.ecmwf.int/codes/grib/param-db/?id=140112. [Online; Accessed 5 November 2022].

[54] Cahill B, Lewis T. Wave period ratios and the calculation of wave power. In: 2nd Marine energy technology symposium METS2014. 2014, p. 1–10.

[55] Khan M, Khalid A, Lughmani WA, Khan MM. A use case of exclusive economic zone of Pakistan for wave power potential estimation. Ocean Eng 2021;237:109664. http://dx.doi.org/10.1016/j.oceaneng.2021.109664.

[56] Lobeto H, Menéndez M, Losada IJ, Hemer M. The effect of climate change on wind-wave directional spectra. Glob Planet Change 2022;213:103820. http://dx.doi.org/10.1016/j.gloplacha.2022.103820.

[57] Caloiero T, Aristodemo F, Ferraro DA. Annual and seasonal trend detection of significant wave height, energy period and wave power in the Mediterranean Sea. Ocean Eng 2022;243:110322. http://dx.doi.org/10.1016/j.oceaneng.2021.110322.

[58] Divinsky BV, Kosyan RD. Spatiotemporal variability of the Black Sea wave climate in the last 37 years. Cont Shelf Res 2017;136:1–19. http://dx.doi.org/10.1016/j.csr.2017.01.008.

[59] Atan R, Goggins J, Nash S. Galway Bay–The 1/4 scale wave energy test site? A detailed wave energy resource assessment and investigation of scaling factors. Renew Energy 2018;119:217–34. http://dx.doi.org/10.1016/j.renene.2017.11.090.

[60] Ulazia A, Penalba M, Ibarra-Berastegui G, Ringwood J, Sáenz J. Reduction of the capture width of wave energy converters due to long-term seasonal wave energy trends. Renew Sustain Energy Rev 2019;113:109267. http://dx.doi.org/10.1016/j.rser.2019.109267.

[61] EMODnet Bathymetry Consortium. EMODnet digital bathymetry (DTM). 2020, URL https://doi.org/10.12770/bb6a87dd-e579-4036-abe1-e649cea9881a.

[62] Theil H. A rank-invariant method of linear and polynomial regression analysis, 3; confidence regions for the parameters of polynomial regression equations. Stichting Math Cent Stat Afdeling 1950;1–16.

[63] Babarit A, Delhommeau G. Theoretical and numerical aspects of the open source BEM solver NEMOH. In: 11th European wave and tidal energy conference, no. 08C1. 2015, p. 1–12.

[64] Saenz-Aguirre A, Saenz J, Ulazia A, Ibarra-Berastegui G. Optimal strategies of deployment of far offshore co-located wind-wave energy farms. Energy Convers Manage 2022;251:114914. http://dx.doi.org/10.1016/j.enconman.2021.114914.

[65] Martinez A, Iglesias G. Wave exploitability index and wave resource classification. Renew Sustain Energy Rev 2020;134:110393. http://dx.doi.org/10.1016/j.rser.2020.110393.

[66] Kamranzad B, Amarouche K, Akpinar A. Linking the long-term variability in global wave energy to swell climate and redefining suitable coasts for energy exploitation. Sci Rep 2022;12(1):14692. http://dx.doi.org/10.1038/s41598-022-18935-w.

[67] Kobayashi S, Ota Y, Harada Y, Ebita A, Moriya M, Onoda H, et al. The JRA-55 reanalysis: General specifications and basic characteristics. J Meteorol Soc Japan Ser II 2015;93(1):5–48. http://dx.doi.org/10.2151/jmsj.2015-001.

[68] Tamarin T, Kaspi Y. The poleward shift of storm tracks under global warming: A Lagrangian perspective. Geophys Res Lett 2017;44:10666–74. http://dx.doi.org/10.1002/2017GL073633.

[69] Rohrer M, Brönnimann S, Martius O, Raible CC, Wild M. Decadal variations of blocking and storm tracks in centennial reanalyses. Tellus A 2019;71:1586236. http://dx.doi.org/10.1080/16000870.2019.1586236.

[70] Thorne PW, Vose RS. Reanalyses suitable for characterizing long-term trends. Bull Am Meteorol Soc 2010;91:353–62. http://dx.doi.org/10.1175/2009BAMS2858.1.

[71] Caloiero T, Aristodemo F, Ferraro DA. Trend analysis of significant wave height and energy period in southern Italy. Theor Appl Climatol 2019;138:917–30. http://dx.doi.org/10.1007/s00704-019-02879-9.

[72] Simonetti I, Cappietti L. Mediterranean coastal wave-climate long-term trend in climate change scenarios and effects on the optimal sizing of OWC wave energy converters. Coast Eng 2022;104247. http://dx.doi.org/10.1016/j.coastaleng.2022.104247.